

Computing a Family of Skeletons of Volumetric Models for Shape Description

Tao Ju¹, Matthew L. Baker², and Wah Chiu²

¹ Washington University, St. Louis, MO

² Baylor College of Medicine, Houston, TX

Abstract. Skeletons are important shape descriptors in object representation and recognition. Typically, skeletons of volumetric models are computed via an iterative thinning process. However, traditional thinning methods often generate skeletons with complex structures that are unsuitable for shape description, and appropriate pruning methods are lacking. In this paper, we present a new method for computing skeletons on volumes by alternating thinning and a novel skeleton pruning routine. Our method creates a family of skeletons parameterized by two user-specified numbers that determine respectively the size of curve and surface features on the skeleton. As demonstrated on both real-world models and medical images, our method generates skeletons with simple and meaningful structures that are particularly suitable for describing cylindrical and plate-like shapes.

1 Introduction

Representing and understanding shapes play central roles in many of today's graphics and vision applications. These applications typically benefit from some form of shape descriptors, one of which is known as skeletons. A skeleton is a compact, medial structure that lies within a solid object [1]. A skeleton of a 2D object consists of 1D (e.g., curve) elements, whereas the skeleton of a 3D object may consist of both 1D and 2D (e.g., surface) elements. A skeleton that captures essential topology and shape information of the object in a simple form is extremely useful in solving various problems such as character recognition, 3D model matching and retrieval, and medical image analysis.

Here we consider computing skeletons of a 3D object consisting of lattice points in a binary volume. While there has been numerous work on 2D skeletonization (see an excellent survey in [2]), methods for computing 3D skeletons are relatively scarce. Skeletonizing volumetric models often utilizes a *thinning* process that iteratively removes deletable object points until a thin, skeletal structure is left. To preserve the object's topology during thinning, deletable points must be *simple* [3,4,5] in that their removal does not invoke topology change. In addition, to prevent shrinking of curves or surfaces that may carry the object's shape information, various types of *curve-end points* or *surface-end points* [3,6,7,8,9,10] can be identified and preserved during thinning. Thinning methods can also be classified as sequential [11], meaning deletable points are identified and removed one after another, or parallel (see review in [12]), meaning all deletable points are collected and removed at once in each thinning iteration.

Unfortunately, the skeletons computed by thinning methods often exhibit a complex structure. For example, Figure 1 (b) shows the result of the parallel thinning method

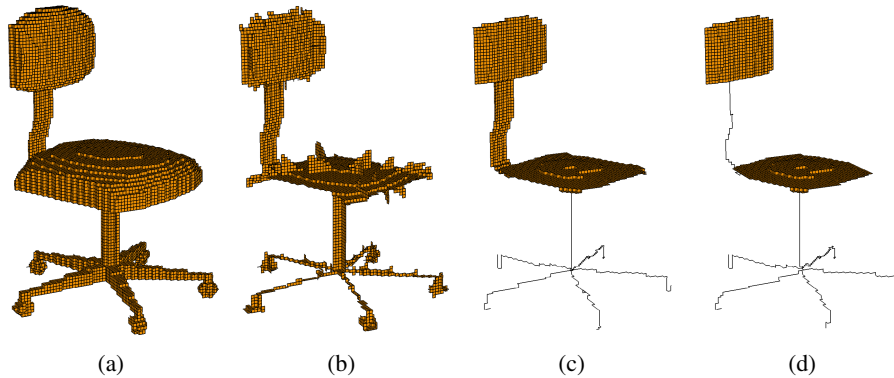


Fig. 1. A volumetric chair model (a), the skeleton computed using the parallel thinning method of Bertrand [9] (b), and two skeletons computed using our method with parameters $d_1 = 20, d_2 = 4$ (c) and $d_1 = 20, d_2 = 7$ (see explanations in Section 3.2)

of Bertrand [9] on the chair model in (a). Note in particular that the spurious surface branches do not provide meaningful information about the original object. Moreover, the chair legs have cylindrical shapes and can be represented in a simpler and more descriptive manner by 1D curves. Typically, a thinning method computes one skeleton for each object, leaving little room for adjustment. Although numerous pruning methods exist for 2D skeletons [13,14], for skeletons of 3D point-set and polygonal models [15,16,17,18,19,20,21] or for removing only curve branches from skeletons of volumetric models [22,23], pruning both redundant curve and surface features from skeletons of volumetric models has not been addressed so far.

Our main contribution is a new method for computing skeletons of a volumetric model by incorporating iterative thinning with skeleton pruning. The core of our method is a simple and efficient pruning algorithm capable of removing redundant curve features as well as surface features from an arbitrary skeleton. Pruning involves morphological erosion and dilation, and is governed by two user-specified parameters that allow flexible control over the size of skeleton curves and surfaces. Pruning and thinning are combined in alternating steps to compute simple, topology-preserving and shape-depicting skeletons. Figure 1 (c,d) give two example skeletons computed using our method with different pruning parameters.

An interesting application that we shall explore is the use of our computed skeletons in describing cylindrical and plate-like shapes. Models composed of these two shapes are not only common in our everyday life, such as chairs and tables, but also appearing often in medical imaging, such as the bone matrix [24,25] and the protein images that we shall see in Section 5. While varying the parameters in our method will produce a large family of skeletons, reasonable choices of parameters yield descriptive skeletons whose curves and surfaces correspond well to the cylindrical and plate-like shape components of the object, as seen in Figure 1 (c,d). In particular, the pruning parameters in our method enable flexible adjustment in the differentiation between cylinders and plates. We note that there have been previous attempts for identifying these two types of shapes directly using an un-pruned skeleton via classifying skeleton points [24,25].

However, as seen in Figure 1 (b), such attempts may easily yield incorrect results due to the complexity of a skeleton computed by thinning.

2 Digital Topology and Discrete Geometry

Here we briefly review basic concepts in digital topology that are fundamental to thinning-based skeletonization algorithms. As part of our own contribution, we follow by introducing several new notions for describing curves and surfaces on volumes.

2.1 Simple Points

We consider a volumetric model as a uniform 3D lattice consisting of *object points* V and *background points* \bar{V} . For topology analysis, we classify the $3 \times 3 \times 3$ neighborhood of each point x into three (overlapping) sets, $N_6(x)$, $N_{18}(x)$ and $N_{26}(x)$, each consisting of points (other than x) that share a common grid edge, face or cell with x . The three sets are illustrated in Figure 2 (a). In addition, we denote $N_k(x, V) = N_k(x) \cap V$.

The topology of the object V is determined by the connectivity of points in V . We regard two points x, y as k -connected if $y \in N_k(x)$ for $k = 6, 18, 26$. In this paper we assume that the object points are 6-connected and the background points are 26-connected, so that the topology of the set V agrees with that of the iso-surface of the whole volume generated by mainstream contouring techniques, such as the Marching Cubes method and its variants [26,27]. In order to maintain topology of V during skeletonization, we follow the result of Bertrand [5] to determine if a point $x \in V$ is *simple* with respect to V , that is, if $V \setminus \{x\}$ preserves the topology of V :

Proposition 1. *Let $s(V)$ denote the set of simple points of V , then $x \in s(V)$ if and only if $c_6(N_6^2(x, V)) = 1$ and $c_{26}(N_{26}(x, \bar{V})) = 1$. Here $c_k(X)$ computes the number of k -connected components in point set X , and*

$$N_6^2(x, V) = N_6(x, V) \cup \bigcup_{y \in N_6(x, V)} M(x, y, V),$$

where $M(x, y, V) = N_{18}(x, V) \cap N_6(y, V)$.

2.2 Discrete Curves and Surfaces

A curve in an object V is a connected collection of object *edges*, each composed of two 6-connected object points, and a surface in V is a connected collection of object *faces*, each composed of four 18-connected object points. In Figure 2 (b,c), edges are shown as dark lines and faces as orange polygons.

Knowledge of curves and surfaces is critical as they are the components of a skeleton that carry shape information of the object. To prevent loss of such information during thinning, it is important to avoid shrinking of the curves and surfaces. While various definitions of curve-end and surface-end points have been proposed in previous work, few are designed for 6-connected objects (except in [9]). In our new definition, a set $S \in N_6(x, V)$ is called *locally 1-manifold* if $S \cup \{x\}$ forms two edges containing x , and

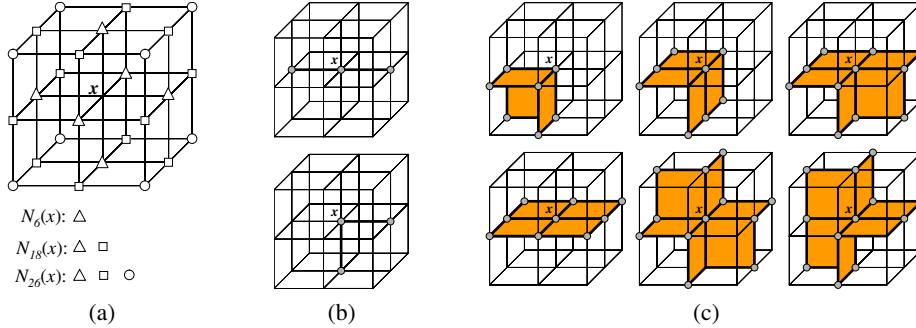


Fig. 2. (a): The 6, 18 and 26 neighborhoods $N_k(x)$. (b): Examples of locally 1-manifold subset of $N_6(x, V)$. (c): Examples of locally 2-manifold subset of $N_{18}(x, V)$.

$S \in N_{18}(x, V)$ is called *locally 2-manifold* if $S \cup \{x\}$ forms a ring of faces containing x that are topologically equivalent to a disk. Figure 2 (b,c) enumerate all rotationally distinct cases of local manifolds. A point $x \in V$ is therefore a *curve-end* (or *surface-end*) point if $N_6(x, V)$ (or $N_{18}(x, V)$) does not contain any locally 1-manifold (or 2-manifold) subset. Intuitively, there exists no curve that passes through a curve-end point, and no surface that completely surrounds a surface-end point. Both curve-end and surface-end points can be efficiently identified as follows (see proof in Appendix A):

Proposition 2. Let $\partial_m(V)$ denote the set of curve-end ($m = 1$) or surface-end ($m = 2$) points of an object V , for any $x \in V$ we have

1. $x \in \partial_1(V)$ if and only if $\#N_6(x, V) < 2$.
2. $x \in \partial_2(V)$ if and only if $r(x, V) = 0$ where

$$r(x, V) = \#N_6^2(x, V) - c_6(N_6^2(x, V)) - \sum_{y \in N_6(x, V)} \#M(x, y, V)$$

Here $\#$ computes set cardinality and $N_6^2(x, V), M(x, y, V)$ are defined in Proposition 1.

Proof

1. By definition, x is not a curve-end point if $N_6(x, V)$ contains more than two points, which form at least two edges with x .
2. First we observe that the quantity $\sum_{y \in N_6(x, V)} \#M(x, y, V)$ equals to the number of edges formed by points in the set $N_6^2(x, V)$. Consider the graph formed by the points and edges in $N_6^2(x, V)$, $r(x, V)$ in fact computes the number of closed rings of edges in the graph. Furthermore, each such ring is a locally 2-manifold subset of $N_{18}(x, V)$. Hence $x \in \partial_2(V)$ if and only if $N_6^2(x, V)$ does not contain any rings, or $r(x, V) = 0$. □

In addition to curve-end and surface-end points, we are also interested in the local neighborhood of each interior point on a curve or surface. An object point y is called a *curve-neighbor* (or *surface-neighbor*) of x if y lies in a locally 1-manifold (or 2-manifold) subset of $N_6(x, V)$ (or $N_{18}(x, V)$). Like end points, we present an explicit characterization of neighbor points (see proof in Appendix A):

Proposition 3. Let $\omega_m(x, V)$ denote the set of curve-neighbor ($m = 1$) or surface-neighbor ($m = 2$) points of $x \in V$, for any $y \in V$ we have

1. $y \in \omega_1(x, V)$ if and only if $y \in N_6(x, V)$ and $\#N_6(x, V) \geq 2$.
2. $y \in \omega_2(x, V)$ if and only if $y \in N_{18}(x, V)$ and $r(x, V) > r(x, V \setminus \{y\})$.

Here $r(x, V)$ is defined in Proposition 2.

Proof

1. By definition, y is a curve-neighbor of x only if y lies in a locally 1-manifold subset of $N_6(x, V)$, which requires both the existence of such a subset, i.e. $\#N_6(x, V) \geq 2$, and that $y \in N_6(x, V)$.
2. From the proof of Proposition 2, we know that $r(x, V)$ counts the number of possible locally 2-manifold subsets of $N_{18}(x, V)$. y lies in a locally manifold subset of $N_{18}(x, V)$ if and only if removing y from V reduces the number of manifold subsets. \square

3 The Algorithms

The skeleton is computed by alternating two morphological operations: thinning and skeleton pruning. For thinning, we adopted the standard iterative paradigm while incorporating our new end-points definition for shape preservation. For pruning, we introduce a simple and effective procedure that extends the dilation and erosion operations often used in image denoising. The algorithms of thinning and pruning are discussed, and the complete method is presented last.

3.1 Iterative Thinning

Thinning begins with a volumetric object V with boundary points $\partial(V)$. Assuming 6-connectivity of the object (as explained in Section 2.1), the boundary is defined as

$$\partial(V) = \{x | x \in V \text{ and } N_6(x, \bar{V}) \neq \emptyset\}$$

Thinning removes each boundary point from V except for *critical* points, whose removal will alter the topology of V or result in loss of shape information. In our context, a critical point x can be either a non-simple point, a curve-end point or a surface-end point. We can write this definition of a critical point as a boolean expression:

$$IsCritical_m(x, V) = x \notin s(V) \text{ or } x \in \partial_m(V)$$

Here, the subscript $m = 0, 1, 2$ determines whether discrete surfaces ($m = 2$) or curves ($m = 1$) in addition to the topology of V are to be preserved during thinning, or only topology information will be preserved ($m = 0$, where we let $\partial_0(V) = \emptyset$).

Note that based on the above definition, a curve-end or surface-end point that forms a small surface bump can be identified as critical points, such as those shown in Figure 3 (a,c) (end-points are drawn as triangles). These bumps are often resulted from discretizing a smooth surface. To distinguish discretization errors from shape features, in

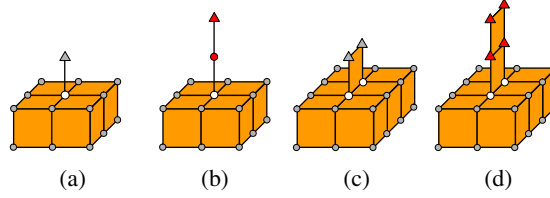


Fig. 3. Defining critical points: A curve-end or surface-end point (shown as triangles) is critical (colored red) only if it is shared by an edge or face that does not contain any non-boundary points (colored white)

practice, we add an additional restriction such that a curve-end (or surface-end) point is critical only if it is contained in an edge (or face) that contains only boundary points. As a result, only curve-end and surface-end points in Figure 3 (b,d) are considered critical.

The pseudo-code of thinning is shown in Figure 4 left. Thinning is performed iteratively. At each iteration, all boundary points are placed in a queue Q and are visited and removed sequentially. Note that program $Thin_m$ takes an extra parameter S , which is a subset of V that will be “protected” during thinning, i.e., no point of S will be removed from V . The use of S will become clear when the complete method is revealed in Section 3.3.

<pre> // Thinning object V while preserving S // m: 0 (topology), 1 (curve), 2 (surface). Thin_m(V, S) Repeat Q ← ∂(V) n ← 0 Repeat while Q ≠ ∅ x ← POP(Q) If x ∉ S and IsCritical_m(x, V) = False V ← V \ {x} n ← n + 1 If n = 0 Return V </pre>	<pre> // Pruning skeleton V with depth d_m // m: 1 (curve), 2 (surface). Prune_m(V, d_m) If d_m ≤ 0 Return V V' ← V \ ∂_m(V) S ← Prune_m(V', d_m - 1) Q ← ∂_m(S) Repeat for all x ∈ Q Repeat for all y ∈ N₁₈(x, V) If y ∈ ω_m(x, V) and y ∉ S S ← S ∪ {y} Return S </pre>
---	--

Fig. 4. Pseudo code for iterative thinning (left) and skeleton pruning (right)

For convenience, we refer to program $Thin_m$ as *surface thinning* ($m = 2$), *curve thinning* ($m = 1$), or *topology thinning* ($m = 0$). Figure 5 shows the result of thinning on three primitive shapes: a sphere, a cylinder and a plate. Observe in particular that surface thinning generates large surfaces for plate-like shapes, while curve thinning results in long curves for cylindrical shapes.

3.2 Skeleton Pruning

Pruning is the process of removing redundant curve or surface features from a skeleton. Examples of redundant features that we wish to remove include short curve branches,

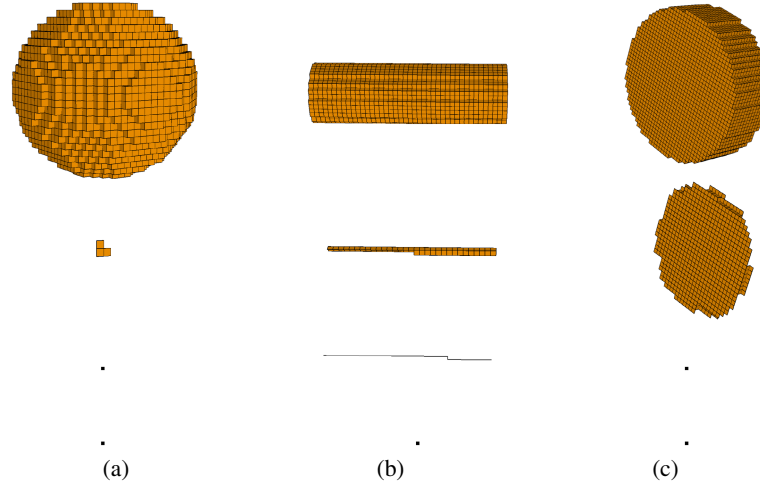


Fig. 5. Volumetric objects (top row) and their skeletons after surface thinning (second row), curve thinning (third row) and topology thinning (bottom row). The black dot represents a single skeleton point.

small surface branches, jagged surface borders and narrow surface bands. Our algorithm extends two morphological operators, namely erosion and dilation, which are often coupled (known as *opening*) in image processing to remove small and thin image artifacts and to smoothen jagged object borders. Whereas image denoising takes place on a 2D or 3D grid, skeleton pruning takes place on discrete curves and surfaces, and hence the two operators are adapted accordingly.

Given a skeleton object V and a super-set $V' \supset V$, our definition of erosion and dilation is based on end-points and neighbor-points introduced in Section 2.2:

$$\begin{aligned} \text{Erode}_m(V) &= V \setminus \partial_m(V) \\ \text{Dilate}_m(V, V') &= V \cup \bigcup_{x \in \partial_m(V)} \omega_m(x, V') \end{aligned}$$

where $m = 1$ or 2 , $\partial_1(V)$, $\partial_2(V)$ are curve-end and surface-end points, and $\omega_1(x, V)$, $\omega_2(x, V)$ are curve-neighbor and surface-neighbor points. In words, erosion retracts V along its curve ($m = 1$) or surface ($m = 2$) border, while dilation expands V towards a larger set V' by growing manifold neighborhoods from the curve ($m = 1$) or surface ($m = 2$) border of V . Note that unlike thinning, erosion and dilation are topology-altering. Figure 6 shows an example of applying two rounds of surface erosion (b,c) followed by two rounds of surface dilation (d,e). The skeleton after i rounds of erosion ($i = 1, 2$) is used as the super-set V' for the $(2 - i)$ th round of dilation.

Observe in Figure 6 that the combination of erosion and dilation has the effect of removing small, narrow features and smoothing borders. Hence we couple the two operators to form pruning, which is recursively defined as

$$\text{Prune}_m(V, d_m) = \text{Dilate}_m(\text{Prune}_m(\text{Erode}_m(V), d_m - 1), V).$$

where $d_m \geq 0$ is the *pruning parameter*, and $\text{Prune}_m(V, 0) = V$.

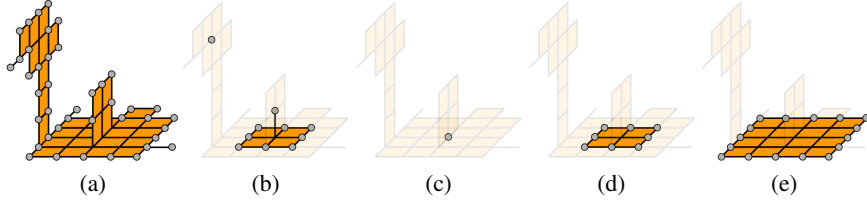


Fig. 6. A skeleton object (a), the result of applying two rounds of surface erosion (b,c), followed by two rounds of surface dilation (d,e). Eroded or dilated points at each step are highlighted.

The pseudo-code of pruning is provided in Figure 4 right. Pruning is performed recursively. At each recursion level, the eroded skeleton $V \setminus \partial(V)$ is first passed to the next level. Given the pruned skeleton S returned from the recursive call, the boundary points of S are then placed in a queue Q and processed sequentially for dilation. For each point in Q , dilation searches within the point's 18-neighborhood for curve-neighbor (or surface-neighbor) points and adds them to S . Note that, instead of storing multiple copies of the skeleton V during recursion, an integer value $d[x]$ can be computed and stored at each point $x \in V$ keeping track of recursion levels. Initially, all $d[x]$ are initialized as ∞ . During recursion, $d[x]$ is first set to the level of recursion where x is eroded, and later reset to ∞ when it is dilated.

Like thinning, we refer to program $Prune_1(V, d_1)$ as *curve pruning* and $Prune_2(V, d_2)$ as *surface pruning*. Examples of pruning can be found as part of Figure 7 on the right, where surface pruning (top) and curve pruning (bottom) are applied with various parameters. Observe that larger values of d_1 remove longer curve branches, while larger values of d_2 remove wider surface bands and produce smoother surface borders. An important feature of our pruning method is that it does not shrink major curves or surfaces as a result of removing noises, similar the effect of opening in image denoising.

3.3 The Complete Method

We have presented two independent algorithms so far: a thinning operation that preserves the topology of the object yet may result in redundant features on the skeleton, and a pruning operation that removes redundant features from a skeleton yet may alter its topology. To create a skeleton that is both topology-preserving and composed of meaningful features, we combine thinning and pruning in alternating steps. Given an initial object V and pruning parameters d_1, d_2 , we compute the final skeleton S in three steps:

Step 1. Extract major surface features by surface thinning followed by surface pruning (Figure 7 top):

$$S \leftarrow Prune_2(Thin_2(V, \emptyset), d_2).$$

Step 2. Extract major curve features by curve thinning followed by curve pruning (Figure 7 bottom):

$$S \leftarrow Prune_1(Thin_1(V, S), d_1).$$

Step 3. Ensure topology preservation through topology thinning:

$$S \leftarrow Thin_0(V, S).$$

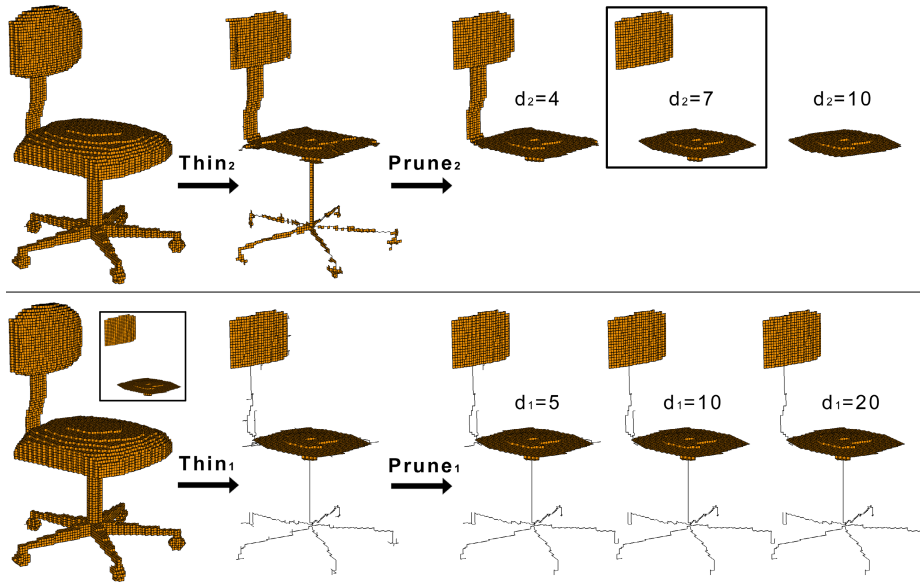


Fig. 7. Step 1 (top) and 2 (bottom) in generating a skeleton. Note that in the second step, curve thinning preserves the surfaces (shown in the insert) computed by the first step.

Note that in each step thinning is applied to the *original* object V . Except for step 1, thinning in both steps 2 and 3 also preserve major surfaces and/or curves computed in the previous step (through the use of the argument S in program $Thin_m(V, S)$). The final thinning step is necessary to ensure a topology-preserving skeleton, as pruning may alternate the topology of the object V .

The combination of thinning and pruning allows a whole spectrum of skeletons being generated by changing the two parameters d_1, d_2 . For example, we can reproduce the result of directly applying surface thinning ($Thin_2(V, \emptyset)$), curve thinning ($Thin_1(V, \emptyset)$) and topology thinning ($Thin_0(V, \emptyset)$) using parameters $\{d_1, d_2\} = \{0, 0\}, \{\infty, 0\}$ and $\{\infty, \infty\}$. More importantly, as observed in Figure 7, reasonable choices of d_1, d_2 would yield skeletons whose curves and surfaces correspond well to cylindrical and plate-like shapes of the original object. In addition, varying the parameters allow the user to adjust the differentiation between these two shape types (Figure 1 is such an example).

4 Results

We demonstrate our skeletonization method on several artificial and scanned models, as shown in Figure 8 and 9. Each model is originally represented in polygonal formats and converted into volumetric forms using the PolyMender software [28]. Observe that our skeleton accurately captures the three structural components of the goblet, which is composed of 2 plates and 1 cylinder. Although the horse and the bunny do not consist of obvious cylinders and plates, the skeletons still provide a descriptive view of its overall shape as well as the difference among local shapes. Note from Figure 9 that varying the

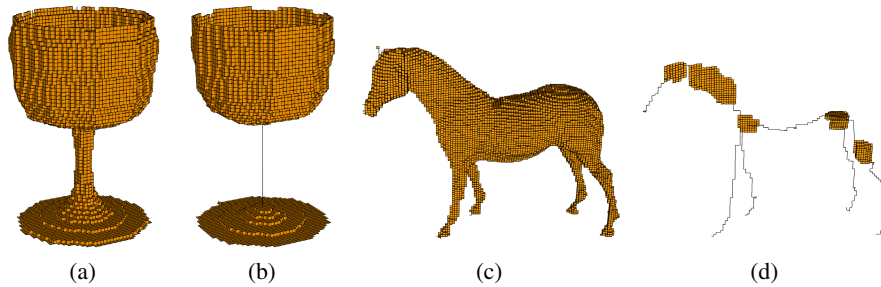


Fig. 8. A goblet (a) and a horse (c) with their skeletons (b,d). Pruning parameters $d_1 = 20$ and $d_2 = 3$ are used in both examples.

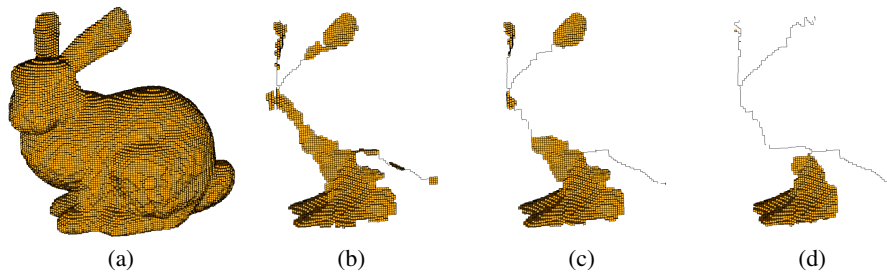


Fig. 9. A bunny model (a) and its skeletons with parameters $\{d_1, d_2\}$ at $\{50, 2\}$ (b), $\{50, 4\}$ (c) and $\{50, 10\}$ (d)

pruning parameter gives multiple choices of skeletons that may be useful in different applications.

We have also applied our method in the bio-medical setting for identifying β -sheet elements from low-resolution protein images. Figure 10 (a) shows protein density models reconstructed from cryo-electron microscopy (cryo-EM). Unlike X-ray crystallography, cryo-EM is capable of imaging large molecular assemblies in nearly native states [29]. However, the drawback of cryo-EM is that the reconstructed model has a much lower resolution (typically 6 to 10 Å) than that of X-ray (less than 3 Å), and resolving atomic details is not possible. Nevertheless, secondary structures of the protein, such as α -helices, β -sheets and loops, are discernable at this resolution and can be recognized as cylinders (loops and α -helices) and curved plates (β -sheets). We applied our method to cryo-EM models, and the resulted skeletons (shown in Figure 10 (c)) differentiate cylindrical and plate-like shapes as skeleton curves and surfaces. Such differentiation allows β -sheets to be identified as skeleton surfaces in an automatic manner. We confirm our result by comparing our skeleton with the actual protein structure revealed by X-ray experiments, shown in Figure 10 (d), where β -sheets are drawn as parallel blue arrows. In contrast, applying Bertrand's parallel technique [9] yields far more surface components on the skeleton than our method, as shown in Figure 10 (b), making it impossible to differentiate plate-like and cylindrical shapes.

In contrast to previous skeletonization algorithms that typically involve one pass of thinning, our method involves three passes of thinning and two passes of pruning. As

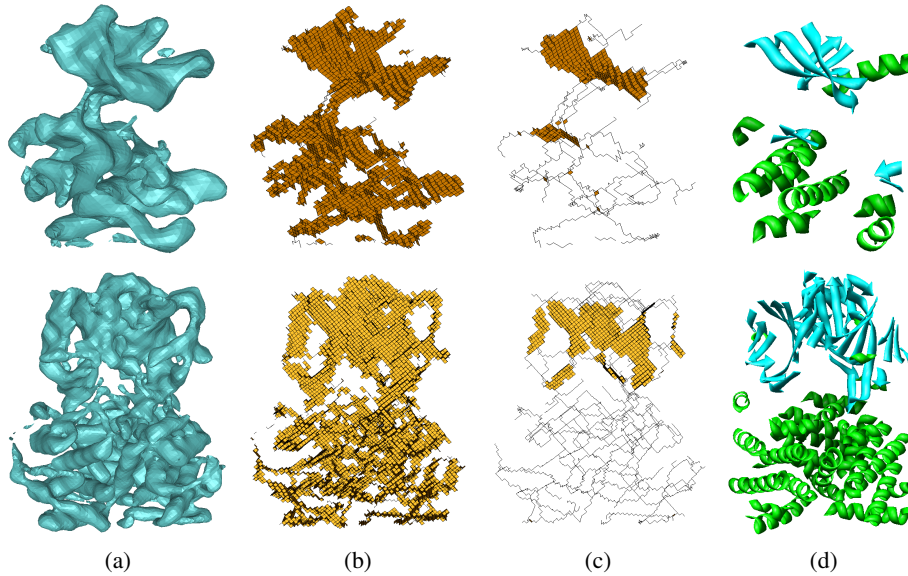


Fig. 10. The iso-surface models of proteins IRK and 1BVP (a), the skeletons computed by [9] (b), the skeletons computed using our method with $d_1 = d_2 = 3$ (c), and the actual structures of these proteins determined by X-ray crystallography (d), where blue stripes denote β -sheets and green spirals denote α -helices. Observe that the skeleton surfaces computed by our algorithm correspond well to the actual β -sheets in the protein structure.

Table 1. Performance of skeletonization for the examples in this paper. The timings are recorded in seconds, and are broken down into various thinning and pruning passes, see Section 3.3.

Model	Grid Size	# Object Voxels	Step 1 (Thin)	Step 1 (Prune)	Step 2 (Thin)	Step 2 (Prune)	Step 3 (Thin)	Total Time	Bertrand [9]
Goblet	64	15911	0.79	0.08	0.24	0.02	0.15	1.28	0.15
Chair	128	34920	1.28	0.28	1.04	0.19	0.65	3.44	1.21
Horse	128	54172	1.69	0.28	1.62	0.18	1	4.77	1.92
Bunny	128	214898	7.12	0.29	5.47	0.19	3.42	16.49	4.94
Protein 1IRK	128	10887	0.47	0.25	0.43	0.17	0.3	1.62	0.31
Protein 1BVP	128	24741	1.4	0.28	0.93	0.17	0.56	3.34	0.45

a result, our method runs slower than most thinning methods, as shown in Table 1, yet still at a reasonable speed. All experiments were run on a PC with Pentium 4 CPU at 1.7GHz and 512MB memory. The timings are broken down into each thinning and pruning pass and are compared with the parallel thinning method of Bertrand [9].

5 Conclusion and Discussion

In this paper, we describe a method for computing a family of topology and shape preserving skeletons of a volumetric model. The method is composed of two algorithms:

iterative thinning and skeleton pruning. Our method allows flexible control over the size of curves or surfaces on the resulting skeletons, which can be used for describing shapes of objects composed of cylindrical and plate-like regions.

As a future direction of research, we are investigating more shape applications, such as segmentation, matching and recognition, using the skeleton generated by our method. In particular, we will explore the use of the skeletons of proteins in fast and accurate fold recognition and comparison, which is an important task demanded by researchers in structural biology. Additionally, we are interested in developing algorithms that automatically determine the appropriate pruning parameters to compute desirable skeletons with minimum or no human input.

References

1. Blum, H.: A transformation for extracting new descriptors of shape. In Wathen-Dunn, W., ed.: *Models for the Perception of Speech and Visual Forms*. MIT Press, Amsterdam (1967) 362–380
2. Lam, L., Lee, S.W., Suen, C.Y.: Thinning methodologies—a comprehensive survey. *IEEE Trans. Pattern Anal. Mach. Intell.* **14** (1992) 869–885
3. Lee, T.C., Kashyap, R.L., Chu, C.N.: Building skeleton models via 3-d medial surface/axis thinning algorithms. *CVGIP: Graph. Models Image Process.* **56** (1994) 462–478
4. Saha, P.K., Chaudhuri, B.B.: Detection of 3-d simple points for topology preserving transformations with application to thinning. *IEEE Trans. Pattern Anal. Mach. Intell.* **16** (1994) 1028–1032
5. Bertrand, G.: Simple points, topological numbers and geodesic neighborhoods in cubic grids. *Pattern Recogn. Lett.* **15** (1994) 1003–1011
6. Tsao, Y.F., Fu, K.S.: A parallel thinning algorithm for 3-d pictures. *Comput. Graphics Image Process.* **17** (1981) 315–331
7. Gong, W., Bertrand, G.: A simple parallel 3d thinning algorithm. In: *ICPR90*. (1990) 188–190
8. Bertrand, G., Aktouf, Z.: A 3d thinning algorithms using subfields. In: *Proceedings, SPIE Conference on Vision Geometry III*. Volume 2356. (1994) 113–124
9. Bertrand, G.: A parallel thinning algorithm for medial surfaces. *Pattern Recogn. Lett.* **16** (1995) 979–986
10. Ma, C.M.: A 3d fully parallel thinning algorithm for generating medial faces. *Pattern Recogn. Lett.* **16** (1995) 83–87
11. Saito, T., Toriwaki, J.: A sequential thinning algorithm for three-dimensional digital pictures using the euclidean distance transformation. In: *Proceedings of the 9th Scandinavian Conference on Image Analysis*. (1995) 507–516
12. Palágyi, K., Kuba, A.: A parallel 3d 12-subiteration thinning algorithm. *Graph. Models Image Process.* **61** (1999) 199–221
13. Attali, D., Sanniti di Baja, G., Thiel, E.: Pruning discrete and semicontinuous skeletons. *Lecture Notes in Computer Science, Image Analysis and Processing* **974** (1995) 488–493
14. Shaked, D., Bruckstein, A.: Pruning medial axes. *Comput. Vis. Image Underst.* **69** (1998) 156–169
15. Ogniewicz, R.L., Kübler, O.: Hierarchic Voronoi skeletons. *Pattern Recognition* **28** (1995) 343–359
16. Attali, D., Montanvert, A.: Computing and simplifying 2d and 3d continuous skeletons. *Comput. Vis. Image Underst.* **67** (1997) 261–273

17. Amenta, N., Choi, S., Kolluri, R.K.: The power crust. In: SMA '01: Proceedings of the sixth ACM symposium on Solid modeling and applications, New York, NY, USA, ACM Press (2001) 249–266
18. Dey, T.K., Zhao, W.: Approximate medial axis as a voronoi subcomplex. In: SMA '02: Proceedings of the seventh ACM symposium on Solid modeling and applications, New York, NY, USA, ACM Press (2002) 356–366
19. Foskey, M., Lin, M.C., Manocha, D.: Efficient computation of a simplified medial axis. In: SM '03: Proceedings of the eighth ACM symposium on Solid modeling and applications, New York, NY, USA, ACM Press (2003) 96–107
20. Tam, R., Heidrich, W.: Shape simplification based on the medial axis transform. In: Proceedings of IEEE Visualization. (2003)
21. Sud, A., Foskey, M., Manocha, D.: Homotopy-preserving medial axis simplification. In: SPM '05: Proceedings of the 2005 ACM symposium on Solid and physical modeling, New York, NY, USA, ACM Press (2005) 39–50
22. Mekada, Y., Toriwaki, J.: Anchor point thinning using a skeleton based on the euclidean distance transformation. In: ICPR '02: Proceedings of the 16 th International Conference on Pattern Recognition (ICPR'02) Volume 3, Washington, DC, USA, IEEE Computer Society (2002) 30923
23. Svensson, S., Sanniti di Baja, G.: Simplifying curve skeletons in volume images. *Comput. Vis. Image Underst.* **90** (2003) 242–257
24. Saha, P., Gomberg, B., Wehrli, F.: Three-dimensional digital topological characterization of cancellous bone architecture. *IJIST* **11** (2000) 81–90
25. Bonnassie, A., Peyrin, F., Attali, D.: Shape description of three-dimensional images based on medial axis. In: Proc. 10th Int. Conf. on Image Processing, Thessaloniki, Greece (2001)
26. Lorensen, W.E., Cline, H.E.: Marching cubes: A high resolution 3d surface construction algorithm. In: SIGGRAPH '87: Proceedings of the 14th annual conference on Computer graphics and interactive techniques, New York, NY, USA, ACM Press (1987) 163–169
27. Natarajan, B.K.: On generating topologically consistent isosurfaces from uniform samples. *The Visual Computer* **11** (1994) 52–62
28. Ju, T.: Robust repair of polygonal models. *ACM Trans. Graph.* **23** (2004) 888–895
29. Chiu, W., Baker, M., Jiang, W., Zhou, Z.: Deriving the folds of macromolecular complexes through electron cryomicroscopy and bioinformatics approaches. *Curr. Opin. Struct. Biol.* **2** (2002) 263–269